# Epstein-Barr virus lytic gene BNRF1 promotes B-cell lymphomagenesis via IFI27 upregulation

Ken Sagou[1, 2], Yoshitaka Sato[1,*], Yusuke Okuno[3], Takahiro Watanabe[1], Tomoki Inagaki[1], Yashiro Motooka[4], Shinya Toyokuni[4], Takayuki Murata[5], Hitoshi Kiyoi[2], Hiroshi Kimura[1,*]

[1]Department of Virology, Nagoya University Graduate School of Medicine, Nagoya, Japan
[2]Department of Hematology and Oncology, Nagoya University Graduate School of Medicine, Nagoya, Japan
[3]Department of Virology, Nagoya City University Graduate School of Medical Sciences, Nagoya, Japan
[4]Department of Pathology and Biological Responses, Nagoya University Graduate School of Medicine, Nagoya, Japan
[5]Department of Virology, Fujita Health University School of Medicine, Toyoake, Japan

*To whom correspondence should be addressed: Yoshitaka Sato (yssato@med.nagoya-u.ac.jp) and Hiroshi Kimura (hkimura@med.nagoya-u.ac.jp)

Running title: BNRF1-IFI27 axis in EBV-driven lymphomagenesis

**Abstract**

Epstein-Barr virus (EBV) is a ubiquitous human lymphotropic herpesvirus that is causally associated with several malignancies. In addition to latent factors, lytic replication contributes to cancer development. In this study, we examined whether the lytic gene BNRF1, which is conserved among gamma-herpesviruses, has an important role in lymphomagenesis. We found that lymphoblastoid cell lines (LCLs) established by BNRF1-knockout EBV exhibited remarkably lower pathogenicity in a mice xenograft model than LCLs produced by wild-type EBV (LCLs-WT). RNA-seq analyses revealed that BNRF1 elicited the expression of interferon-inducible protein 27 (IFI27), which promotes cell proliferation. IFI27 knockdown in LCLs-WT resulted in excessive production of reactive oxygen species, leading to cell death and significantly decreased their pathogenicity *in vivo*. We also confirmed that IFI27 was upregulated during primary infection in B-cells. Our findings revealed that BNRF1 promoted robust proliferation of the B-cells that were transformed by EBV latent infection via IFI27 upregulation both *in vitro* and *in vivo*.

**Keywords: EBV, lytic, BNRF1, LCLs, IFI27, ROS**

## Author summary

Virus-infected cells must overcome several anti-viral host responses for stable growth. The human oncogenic herpesvirus Epstein-Barr virus (EBV) carries the genes with anti-apoptotic and proliferative functions. In this study, we demonstrated the role of the EBV protein BNRF1 in the growth resilience of B-cells infected with EBV. BNRF1 induced the expression of interferon-inducible protein 27 (IFI27), driving the proliferation of infected cells. IFI27 knockdown elicited the over production of reactive oxygen species, causing a fragile growth of both EBV-infected and EBV-transformed cells. Furthermore, disruption of the BNRF1-IFI27 axis reduced the pathogenicity of lymphoblastoid cell lines in a mouse xenograft model. These results provide insights into the neoplastic progression of EBV-infected cells and therapeutic targets against EBV-infected cells.

## Introduction

Epstein-Barr virus (EBV) is a ubiquitous human lymphotropic herpesvirus that is causally associated with several malignancies including Burkitt lymphoma, Hodgkin lymphoma, a part of diffuse large B-cell lymphoma (DLBCL), post-transplant lymphoproliferative disorders, T/NK cell lymphoma, and nasopharyngeal carcinoma [1, 2]. EBV establishes latent infection in B cells, in which the virus expresses latent factors rather than producing infectious particles. These EBV factors transform primary B cells into lymphoblastoid cell lines (LCLs) *in vitro*. EBV-mediated suppression of apoptosis plays critical roles in LCL growth and survival [3]. In addition to latent factors, accumulating evidence indicates that lytic replication, the process that generates new virus progeny by viral lytic proteins, contributes to cancer development [4-6].

The EBV tegument protein BNRF1 is an abundant protein in the virion [7], and it exerts multiple effects. BNRF1 homologs are present in all gamma-herpesviruses such as KSHV ORF75 [8] but absent in alpha- and beta-herpesviruses. BNRF1 disrupts ATRX/Daxx complexes to prevent the loading of repressive H3.3 histones onto incoming EBV genomes [9]. BNRF1 knockout (KO) impairs the expression of EBNA2 during the earliest stages of EBV infection in B-cells [9, 10]. BNRF1 enables efficient viral replication by targeting SMC5/6 cohesin complexes to a ubiquitin-proteasome pathway [11]. Furthermore, BNRF1 induces centrosome amplification, leading to chromosomal instability even without establishing chronic infection [12]. Although BNRF1-mediated chromosomal instability is expected to contribute to the initial development of cancer [13], the role of BNRF1 in oncogenesis *in vivo* remains unclear.

In this study, we found that LCLs established by BNRF1-KO EBV exhibited remarkably lower pathogenicity in a mice xenograft model than LCLs produced using wild-type EBV (LCLs-WT). BNRF1 elicited the expression of interferon-inducible protein 27 (IFI27), which promotes cell proliferation [14-19]. The knockdown of IFI27 in LCLs-WT significantly reduced their pathogenicity *in vivo*.

## Results

### *BNRF1 enhanced the frequency of tumor formation in a mouse xenograft model*

To elucidate the roles of BNRF1 in tumor formation, we first generated a BNRF1-KO mutant-BAC (dBNRF1-rEBV) and revertant EBV-BAC (dBNRF1rev-rEBV) from WT EBV-BAC (WT-rEBV), as presented in Fig. 1A. These EBV-BACs were analyzed by Sanger sequencing and restriction digestion with *BamH*I or *EcoR*I, followed by agarose gel electrophoresis (Fig. 1A and 1B). We performed these full bacmid sequencing by Nanopore technology and confirmed no off-target mutation among these rEBVs (S1 Fig.). Subsequently, we established HEK293T/WT-rEBV, HEK293T/dBNRF1-rEBV, and HEK293T/dBNRF1rev-rEBV cells carrying each recombinant EBV, and viruses produced from these cells were named EBV-WT, EBV-dBNRF1, and EBV-dBNRF1rev, respectively.

BNRF1 KO was also confirmed by immunoblotting (Fig. 1C). The expression of glycoprotein B, a late gene, was not affected by the introduction of a stop mutation in the BNRF1 gene (Fig. 1C). BNRF1 KO did not affect viral DNA synthesis (Fig. 1D). Consistent with previous reports [9, 10], the infectivity of the BNRF1-KO virus was significantly lower than that of EBV-WT and EBV-dBNRF1rev after normalization to the EBV DNA copy number (Fig. 1E). The transformation efficiency of EBV-dBNRF1 was approximately 80-fold lower than those of EBV-WT and EBV-dBNRF1rev (Fig. 1F). These findings coincided with the reported phenotype of the EBV mutant lacking the BNRF1 gene [10].

BNRF1 protein induces chromosomal instability via centrosome amplification without establishing a chronic infection [12], suggesting its contribution to tumor development. However, the role of BNRF1 in pathogenesis *in vivo* remains obscure. To examine this, we established LCLs via recombinant EBV-WT or EBV-dBNRF1 infection of peripheral blood mononuclear cells (PBMCs) isolated from a healthy donor (LCLs-WT and LCLs-dBNRF1, respectively) and then evaluated these LCLs in an *in vivo* mouse model of B-cell lymphoma [20]. When injected intraperitoneally into 6-week-old

NOD/Shi-scid-IL2Rγ$^{null}$ immunodeficient mice (NOG) mice, LCLs-dBNRF1 exhibited remarkably lower pathogenicity than LCLs-WT. LCLs-dBNRF1 did not form lymphomas, and all mice survived until day 70 after inoculation (Fig. 1G). The tumors that developed in LCLs-WT-injected mice expressed LMP1 and EBER (Fig. 1H). Interestingly, the viral load in the blood of mice with LCLs-dBNRF1 was detected at 42 days post-inoculation but at low levels, and subsequently tapered at 77 days post-inoculation (S2 Fig.). These findings imply that disruption of the BNRF1 gene abrogated the pathogenicity of LCLs *in vivo* due to the fragile growth of LCLs-dBNRF1. It should be noted that LCLs-dBNRF1 formed tumors in 5-week-old NOG mice (S3 Fig.).

***Loss of BNRF1 reduced LCL survival***

Next, we characterized each LCL *in vitro*. EBNA1, EBNA2, LMP1, and BZLF1 expression did not significantly differ among LCLs-WT, LCLs-dBNRF1, and LCLs produced by EBV-dBNRF1rev (LCLs-dBNRF1rev; Fig. 2A). Of note, the numbers BZLF1$^+$ and BZLF1$^+$/glycoprotein B$^+$ cells showing spontaneous lytic reactivation [21] were comparable among these LCLs (S1 Table).

However, the growth rate of LCLs-dBNRF1 was significantly lower than those of LCLs-WT and LCLs-dBNRF1rev (Fig. 2B). We further assessed the growth properties of LCLs-dBNRF1 with or without serum deprivation using the 3-(4,5-dimethylthiazol-2-yl)-5-(3-carboxymethoxyphenyl)-2-(4-sulfophenyl)-2H-tetrazolium, inner salt (MTS) assay and annexin V/7-aminoactinomycin D (7-AAD) (Fig. 2C and 2D, respectively). As shown in Fig. 2C, LCLs-dBNRF1 exhibited growth delay. Serum deprivation enhanced this growth phenotype (Fig. 2C). The annexin V/ 7-AAD assay revealed that BNRF1-KO increased cell death (Fig. 2D).

To examine whether BNRF1 is responsible for this phenotype of LCLs-dBNRF1, we performed trans-complementation analyses. Exogenous HA-tagged BNRF1 was expressed in LCLs-dBNRF1 via lentivirus-mediated transduction (Fig. 2E). The exogenous expression of BNRF1-HA enhanced cell proliferation (Fig. 2F) and decreased

cell death under serum deprivation (Fig. 2G), indicating the pivotal role of BNRF1 in LCL growth.

***Expression of the BNRF1 gene in LCLs***

To investigate the expression of BNRF1 in LCLs, we performed immunoblotting with the anti-BNRF1 antibody. As shown in S4 Fig., we could not detect the protein encoded by BNRF1. However, owing to the low sensitivity of the antibody, the possibility that BNRF1 is expressed in LCLs cannot be excluded. Thus, we measured the levels of RNA encoding BNRF1 using qRT-PCR analysis and detected BNRF1-mRNA in LCLs (Fig. 3). Lytic replication is spontaneously detected in a small fraction of LCLs. To address the expression of BNRF1 in the B-cells latently infected with EBV, LCLs were treated with ganciclovir to inhibit the lytic replication of EBV [22]. Equal levels of BNRF1-mRNA were detected with or without ganciclovir treatment (Fig. 3), suggesting that BNRF1 was expressed in most LCLs rather than in small population supporting the lytic cycle.

Compared with LCLs, BNRF1 expression was lower in Akata/EBV-EGFP cells (Fig. 3). The growth of Akata/EBV-EGFP was not dependent on EBV, because its parental Akata(-) cell is a cell line established from Burkitt lymphoma. These findings support the role of BNRF1 in overcoming fragile growth.

***BNRF1 induced IFI27 expression***

To elucidate the mechanisms underlying the BNRF1-mediated growth advantage of LCLs, we compared gene expression profiles between LCLs-WT and LCLs-dBNRF1. The upregulated genes are listed in Fig. 4A and S2 Table. Consistent with our findings in Fig.2, GO term analysis showed that the growth was stimulated in LCLs-WT compared with LCLs-dBNRF1 (S5 Fig.). Of note, obvious differences in EBV gene expression were not observed between LCLs-WT and LCLs-dBNRF1 (S3 Table).

To decrease bias and further narrow BNRF1-responsive genes, we established Akata(-) cells expressing HA-tagged BNRF1 in a tetracycline-inducible manner (Tet-

BNRF1-HA/Akata(-) cells; Fig. 4B) and then performed RNA-seq analysis using Tet-BNRF1-HA/Akata(-) cells with or without doxycycline (Dox) induction (Fig. 4C and S4 Table). As illustrated in Fig. 4D, IFI27 was universally selected as a BNRF1-responsive gene in both BNRF1-KO LCLs and BNRF1-expressing Akata(-) cells. Otofelin (OTOF) was excluded as a candidate because of its low expression in both LCLs and Akata(-) cells. We validated the elevated expression level of IFI27 in LCLs-WT compared to that in LCLs-dBNRF1 by quantitative real-time reverse transcription-PCR (RT-qPCR; Fig. 4E).

In addition, our previous time-course analysis of RNA-seq data from PBMCs infected with wild-type EBV indicated that the mRNA expression of BNRF1 and IFI27 similarly elevated from 4 dpi (S6 Fig.) [23]. It should be noted that IFI27 is upregulated in clinical samples isolated from patients with DLBCL, which is sometimes associated with EBV (GEPIA2 database [24]; Fig. 4F).

A previous study revealed that the expression of IFI27 was induced by STAT1, independent of the STAT1 phosphorylation [25]. We confirmed that BNRF1 upregulated STAT1 in Akata(-) cells (Fig. 5A). However, several EBV latent proteins can upregulate STAT1 [26, 27] to maintain the latency in EBV-transformed cells [28]. As shown in Fig. 5B, LCLs-WT and LCLs-dBNRF1 express STAT1 to the same level, suggesting that the mechanism for the downregulation of IFI27 by BNRF1-KO has. To uncover the mechanisms, further study is required.

***IFI27 enhanced the survival of LCLs-dBNRF1***

To investigate the impact of IFI27 on LCLs, IFI27 was transduced into LCLs-dBNRF1 using lentiviral vectors, and IFI27-expressing cells were selected with blasticidin (Fig. 6A). IFI27 overexpression in LCLs-dBNRF1 significantly stimulated cell proliferation and decreased the rate of cell death (Fig. 6B and 6C).

***IFI27 knockdown reduced the pathogenicity of LCLs in a mouse xenograft model***

We also assessed the effect of IFI27-knockdown (KD) in LCLs-WT. The IFI27 mRNA expression in LCLs-WT expressing shIFI27 (shIFI27/LCLs-WT) was 75% lower than the control level (shScramble/LCLs-WT; Fig. 7A). Consistent with effects of IFI27 overexpression (Fig. 6), IFI27 knockdown in LCLs-WT significantly decreased the growth rate (Fig. 7B and 7C) and increased the rate of cell death (Fig. 7D). These findings highlight the role of IFI27 in EBV-transformed cells *in vitro*.

To evaluate the importance of IFI27 to pathogenicity *in vivo*, we inoculated shIFI27/LCLs-WT or shScramble/LCLs-WT into 5-week-old immunodeficient NOG mice intraperitoneally and observed these xenografted mice. As presented in Fig. 7E, IFI27-KD increased significantly the survival rate of xenografted mice. These results indicated the roles of IFI27 in tumor development *in vivo*.

***BNRF1-KO or IFI27-KD induced reactive oxygen species production***

Recently, IFI27 has been linked to mitochondrial metabolism through fatty acid oxidation (FAO) in adipocytes [29]. During ATP synthesis, mitochondria generate reactive oxygen species (ROS) as an intrinsic by-product [30, 31]. Based on the finding that FAO produces higher ROS level than glucose oxidation [32], we assessed ROS production in LCLs-WT and LCLs-dBNRF1. As shown in Fig. 8A, the level of ROS was higher in LCLs-dBNRF1. Treatment with N-acetyl cysteine (NAC), an antioxidant, stimulated the growth of LCLs-dBNRF1 and decreased cell death (Fig. 8B and 8C), suggesting that ROS were responsible for the fragile growth by BNRF1-KO. Excessive ROS cause insufficient ATP production [33]. Indeed, LCLs-dBNRF1 produced less ATP than LCLs-WT (Fig. 8D).

Similar to LCLs-dBNRF1, the KD of IFI27 elicited ROS production (Fig. 8E). As expected, NAC rescued the phenotype of shIFI27/LCLs-WT (Fig. 8F and 8G). The level of ATP was reduced by IFI27-KD (Fig. 8H). These data indicate that the BNRF1-IFI27 axis collateralizes the robust growth of EBV-transformed cells through efficient ATP production and ROS scavenging.

As shown in Fig. 8I, ATP production was slightly but significantly reduced by the

treatment with etomoxir, an inhibitor of FAO [34], suggesting that FAO was an energy source for LCLs. Simultaneously, we cannot rule out the possibility that IFI27 controls mitochondrial metabolism through not only FAO but also other pathways.

***IFI27 promoted the growth of EBV-infected B cells during primary infection***

The finding that a large amount of BNRF1 contained in virions is transferred to B-cells during EBV infection [7] suggests that the BNRF1-IFI27 axis modulates the growth of EBV-infected cells during primary infection. In fact, recombinant EBV devoid of BNRF1 transformed primary B-cells much less efficiently than EBV-WT [10]. To explore this possibility, we compared the mRNA expression of IFI27 between B-cells infected with EBV-WT and EBV-dBNRF1. As shown in Fig. 9A, rEBV-dBNRF1 did not induce IFI27 expression 7 days after EBV infection.

Furthermore, we assessed the effect of IFI27 on EBV infection using B-cells expressing shIFI27. IFI27 expression was suppressed in EBV-infected B-cells in the presence of shIFI27 (Fig. 9B). The growth curve demonstrated that IFI27-KD inhibited the proliferation of EBV-infected B-cells (Fig. 9C). We also confirmed that the growth of EBV-infected B-cells at 10 days post-infection (dpi) was significantly suppressed by shIFI27 (Fig. 9D). These findings suggested that BNRF1 protein-mediated IFI27 expression contributed to the growth of infected cells during EBV-mediated transformation.

## Discussion

Accumulating evidence has revealed the role of the EBV lytic cycle in cancer development [6], although the precise mechanisms by which the lytic cycle promotes tumor formation and development remain obscure. Intriguingly, progeny production is not required for these processes [12, 20, 35, 36], indicating that the tumor-associated state of EBV is abortive lytic replication and the lytic genes function not only in genomic replication but also in EBV-driven tumor formation and development. EBV encodes

several anti-apoptotic proteins, most of which function in latently infected cells [37]. In this study, we found that abrogation of the EBV major tegument protein BNRF1 resulted in fragile growth in transformed B-cells, leading to a remarkable reduction of the EBV-associated tumor formation in a mouse xenograft model. BNRF1 cell-autonomously induced the expression of IFI27, which ensured robust cell proliferation. In addition, the loss of BNRF1 decreased the transformation activity of primary B-cells as described previously [10]. We also revealed that IFI27 supports the growth of EBV-infected cells during B-cell transformation. The epidemiological findings that pyothorax-associated lymphoma, which is strongly associated with EBV, expresses IFI27 mRNA [38] supports our findings, although the expression of BNRF1 in that lymphoma has not been assessed. Therefore, the BNRF1-IFI27 axis was required for the EBV-mediated tumor formation and development.

IFI27, which is stably induced by type I interferon [39], belongs to the FAM14 family of protein carrying the ISG12 motif [39]. Human IFI27 is considered a transmembrane protein [40, 41]. Previous studies demonstrated that IFI27 enhanced DNA-damage induced apoptosis. This pro-apoptotic effect of IFI27 is canceled by Bcl-2 co-expression [39, 42]. EBV regulates intrinsic apoptosis in infected cells by inducing Bcl-2 expression via LMP1 [43] and expressing viral Bcl-2 proteins, BHRF1, and BALF1 [44, 45]. Over the past decade, IFI27 has been reported to promote tumor cell growth and migration in several cancers [14-19]. Furthermore, recent studies have shown that IFI27 regulates mitochondrial metabolism and thermogenesis in adipocytes [29, 46]. Herein, we demonstrated that perturbation of the BNRF1-IFI27 axis impaired ROS scavenging and ATP production (Fig. 8). Although IFI27 promotes mitochondrial bioenergetics upon cold stress by facilitating FAO in adipocytes [29], an inhibitor of FAO reduced ATP production in LCLs, but was not completely inhibited (Fig. 8I), suggesting that IFI27 controlled mitochondrial metabolism and energy homeostasis in LCLs using not only FAO but also other energy sources. Indeed, the genetic ablation of IFI27 causes broad repression of mitochondrial gene expression [46] and a decrease in the number of mitochondrial cristae

[29]. Abnormal mitochondrial morphology is correlated with ROS production [47]. The underlying molecular mechanism by which IFI27 promotes the cell growth and survival of LCLs remains an open question, and further study is required. We speculate that EBV-infected cells require the IFI27-mediated growth resilience to overcome stresses such as anti-viral responses upon primary infection, and hypoxic and hypovascular circumstances in the tumor.

EBV seroprevalence increases with age. Approximately 95% of healthy adults are infected with EBV [48]. BNRF1 is a major EBV antigen in EBV-seropositive healthy donors [49]. Interestingly, CD8+ T cell clones raised against the tegument protein BNRF1 recognize latent growth-transforming B-cells [50], implying the expression of BNRF1 protein in a latent phase. Consistently, we could detect the mRNA encoding BNRF1 in the latently infected B-cells, although the BNRF1 protein was not detected (Fig. 3 and S4 Fig.). It should be noted that BNRF1 is categorized as a late gene in HEK293/EBV cells [51]. Our findings highlighted the role of BNRF1 in the latent cycle in infected B-cells.

We could not eliminate the possibility that BNRF1 proteins were transferred from the occasional lytic-induced cells to the latently infected cells via extracellular vesicles (EVs) such as exosomes because BNRF1 proteins were incorporated into EVs [52].

This study had several limitations. First, we evaluated IFI27 expression by RT-qPCR, but we did not detect endogenous IFI27 protein because of the limitations of commercial antibodies against IFI27. Second, our results must be confirmed using clinical samples. The information on whether IFI27 is upregulated in EBV-associated tumors requires further investigation. Likewise, the downstream process of IFI27-mediated growth should be intensively studied. These findings will shed light on a potential therapeutic target in EBV-driven transformed cells.

In summary, BNRF1, an EBV lytic gene product, supports the survival of latent growth-transforming B-cells infected with EBV via upregulation of IFI27 both *in vitro* and *in vivo*. BNRF1 KO or IFI27 knockdown decreased the pathogenicity of LCLs in a mouse xenograft model. Our findings provided insights into the growth resilience of

EBV-infected cells via the BNRF1-IFI27 axis.

## Methods

### *Cell culture*

HEK293T and HEK293T/EBV cells were grown in DMEM (Sigma-Aldrich, St. Louis, MO, USA) supplemented with 10% FBS. Akata(-) cells, Akata/EBV-EGFP [53], and LCLs established by recombinant EBV infection were maintained in RPMI 1640 supplemented with 10%-15% FBS. AGS/EBV-EGFP cells (kindly gifted by Hironori Yoshiyama) [54] were grown in RPMI 1640 medium containing 10% FBS and 750 μg/mL G418 [55].

### *Plasmids*

The expression vectors pcDNA-BZLF1 and pcDNA-gB were reported previously [56]. Lentiviral expression constructs of tetracycline-inducible BNRF1-HA, shRNA for IFI27, and control shRNA (pLV-Tet3G and pLV-TRE-BNRF1-HA, pLV-shIFI27-T2A-mCherry, and pLV-shScramble-mCherry) were generated by VectorBuilder (Chicago, IL, USA). To express C-terminal HA-tagged BNRF1 (BNRF1-HA) or Flag-tagged IFI27 (IFI27-Flag), the fragments were cloned into the CSII-CMV-MCS-IRES2-Bsd vector (a gift from Dr. Horoyuki Miyoshi, RIKEN BioResource Center, Wako, Japan). The inserted DNA sequence of each vector was confirmed by direct DNA sequencing.

### *Construction of the dBNRF1 EBV-BAC genome*

The original EBV-BAC (B95-8 strain) was kindly provided by Dr. W. Hammerschmidt [57]. To construct dBNRF1-rEBV and revertant dBNRF1rev-rEBV, homologous recombination was performed in *Escherichia coli* to generate the C429A mutation in the BNRF1 ORF and restore the wild-type sequence, as described previously [56]. The oligonucleotides used for the series of recombination are presented in Table 1. The targeted recombination and full bacmid sequence were confirmed by Sanger and

Nanopore sequencing, respectively (Eurofins Genomics Japan, Tokyo, Japan). HEK293T cells were transfected with recombinant EBV using Fugene 6 reagent (Promega, Wisconsin, USA) and cultured with 150 μg/mL hygromycin B (Takara, Shiga, Japan). After 2 weeks post-transfection, hygromycin-resistant and green fluorescent protein (GFP)-positive cell colonies were cloned as HEK293T/EBV lines for further analyses.

***Establishment of LCLs***

HEK293T cells having recombinant EBV were transfected with the BZLF1 and gB expression plasmids using polyethylenimine (Polysciences, Warrington, PA, USA). Three days after transfection, supernatants from HEK293T/WT-rEBV, HEK293T/dBNRF1-rEBV, or HEK293T/dBNRF1rev-rEBV were harvested; passed through 0.45 μm filters; ultracentrifuged at 100,000 × g for 1.5 h; and used as a virus stock. EBV-negative Akata(-) cells were infected with the virus, and GFP-positive cells were counted using Fortessa X-20 (Becton Dickinson, Franklin Lakes, NJ, USA) to measure the viral titer. LCLs-WT, LCLs-dBNRF1, and LCLs-dBNRF1rev were established as described previously [20]. The Institutional Review Board of Nagoya University Graduate School of Medicine approved this study.

***Lentiviral transduction***

Lentiviruses for LCLs were produced by co-transfecting HEK293T cells with pCMVR8.74 (a gift from Dider Trono and Yasuo Aiumi; #22036, Addgene, Watertown, MA, USA), phCMV-GALV-MTR (a gift from Daniel Hodson; #163612, Addgene), and a third plasmid (CSII-BNRF1-HA, CSII-CMV-MCS-IRES2-Bsd, CSII-IFI27-Flag, pLV-shIFI27-T2A-mCherry, or pLV-shScramble-mCherry). Lentiviruses for Akata(-) cells were produced by co-transfecting HEK293T cells with pCMVR8.74, pCMV-VSV-G (a gift from Bob Weinberg; #8454, Addgene), and pLV-Tet3G or pLV-TRE-BNRF1-HA.

LCLs were infected with the lentiviruses by spinoculation at 1500 × g for 1.5 h in the presence of 5 μg/mL polybrene (VectorBuilder). After incubation for 3 h, LCLs were

resuspended in a fresh medium. At 3 dpi, infected LCLs were incubated with 10 μg/mL blasticidin for at least 10 days.

To establish Tet-BNRF1-HA/ Akata(-) cells inducibly expressing BNRF1-HA, Akata(-) cells were infected with a lentivirus carrying the Tet3G cassette in the presence of 5μg/mL polybrene, and the next day, the culture medium was replaced with fresh medium containing 150 μg/mL hygromycin. After 14 days of culture, cells were infected with a lentivirus carrying the TRE-BNRF1-HA cassette as previously described, and maintained in the presence of 10 μg/mL blasticidin and 150 μg/mL hygromycin.

***EBV infection in shRNA-transduced B cells***

Primary B cells were isolated using EasySep human CD19 positive selection kit II (Veritas, Tokyo, Japan) from healthy donor PBMCs according to the manufacturer's instructions. Isolated B cells were infected with lentiviruses by spinoculation at 1,500 × g for 1.5 h on plates coated with RetroNectin according to the manufacturer's instructions (TaKaRa). Three hours after spinoculation, cells were infected with EBV-EGFP [58] at a multiplicity of infection of 1. Infected B cells were incubated with 10 μg/mL blasticidin at 3 dpi.

***Antibodies, immunoblotting, and flow cytometry***

Anti-BNRF1 was kindly provided by Dr. Lieberman [59], and anti-BZLF1 antibody was purchased from Santa Cruz Biotechnology (Santa Cruz, CA, USA). Polyclonal antibodies against BMRF1, BALF4 (glycoprotein B), and LMP1 were described previously [56]. Anti-STAT1 (#9172), anti-phospho-STAT1 (Tyr701) (#9171), and anti-GAPDH (#5174) antibodies were obtained from Cell Signaling Technology (Danvers, MA, USA). Anti-STAT2 (#693302) and anti-phospho-STAT2 (Tyr631) (#619851) antibodies were purchased from Biolegend. Anti-HA antibody (3F10) (#11867423001)and anti-Flag antibody (M2) (F1804) were purchased from Sigma-Aldrich.

Immunoblotting was performed as described previously [60]. Densitometry was

389 performed using ImageJ.

390 For surface staining, cells were incubated with anti-glycoprotein B antibody before
391 fixation. Then cells were stained with Alexa 647-anti-mouse IgG (A-21235;
392 ThermoFisher Scientific, Waltham, USA) on ice for 30 min. Antibody-stained cells were
393 fixed overnight with 4% paraformaldehyde at 4 °C. Subsequently, cells were treated with
394 0.1% Triton-X100/PBS at room temperature for 10 min. Cells were then stained further
395 with PE-anti-BZLF1 antibody (sc-53904 PE; Santa Cruz Biotechnology) on ice for 30
396 min. Cells were analyzed using a BD Fortessa X-20.

397

398 ***Annexin V/7-AAD assay***

399 The death of LCLs was evaluated by flow cytometry using allophycocyanin annexin V
400 (Biolegend, San Diego, CA, USA) and 7-AAD (Becton Dickinson) according to the
401 manufacturer's instructions.

402

403 ***Cell viability assay (MTS assay)***

404 Cell viability was measured using Cell Titer 96 Aqueous One Solution (MTS reagent;
405 Promega) as described previously [61]. The absorbance was measured at 490 nm on a
406 Rainbow plate reader (Tecan Japan, Kawasaki, Japan).

407

408 ***Quantification of viral DNA***

409 Viral DNA in replicating cells or whole blood of NOG mice was quantified by
410 quantitative real-time PCR (qPCR) as described previously [62].

411

412 ***RT-qPCR***

413 Total RNA was purified using TriPure isolation reagent (Sigma-Aldrich) according to the
414 manufacturer's instructions. Total RNA was subjected to RT-qPCR using One Step TB
415 Green PrimeScript RT-PCR Kit II (Takara) and real-time PCR system 7500 Fast Dx
416 (ThermoFisher Scientific). The primers used for RT-qPCR are presented in Table 2.

***RNA sequence***

Tet-BNRF1/Akata(-) cells cultured with or without 1μg/mL Dox for 2 days, LCLs-WT, and LCLs-dBNRF1 were harvested and total RNA was extracted using an RNeasy mini kit (Qiagen, Hilden, Germany). The evaluation of RNA quality, RNA-seq library preparation, Illumina sequencing, and data preprocessing were performed as described previously [20].

***B cell transformation assay.***

The transformation assay was performed as described previously [63].

***Xenograft experiments using LCLs.***

Either five- or six-week-old female NOG mice (Central Institute for Experimental Animals, Kawasaki, Japan) were inoculated intraperitoneally with $2 \times 10^5$ LCLs suspended in 200 μL of phosphate-buffered saline. Mice survival was the primary endpoint, and mice were sacrificed according to ethical guidelines if their weight decreased by more than 15% versus the basal weight, remarkable ruffled fur was observed, all mice of either group died, or mice were alive on day 70 after LCL inoculation, whichever came first. Tumor formation was assessed in all mice at autopsy.

All animal experiments were approved by the University Committee under the Guidelines for Animal Experimentation at Nagoya University.

Immunohistochemical staining of LMP was performed using an anti-LMP antibody (M0897; Agilent, Santa Clara, CA, USA) and a Leica BOND-MAX (Leica, Bannockburn, IL, USA) with BOND Polymer Detection (ds9800; Leica). During the blocking phase, endogenous mouse tissue IgG was blocked by incubation with an anti-IgG antibody (ab6668; Abcam, Cambridge, UK) at a concentration of 0.1 mg/mL at room temperature for 1 h. EBER-ISH was performed in Kotobiken Medical Laboratories (Tokyo, Japan) as described previously [64].

### *Intracellular ROS and extracellular ATP Assays*

Cellular ROS levels were measured using the Cellular ROS Assay kit (ab186029; Abcam) in accordance with the manufacturer's instructions. Extracellular ATP levels were measured using an ATP Assay Kit-Luminescence (#346-09793; Dojindo, Kumamoto, Japan) in accordance with the manufacturer's instructions, with a SpectraMax id5 (San Jose, CA). *N*-Acetyl-L-cysteine (A9165; Sigma-Aldrich) was purchased from Merck (Darmstadt, Germany). Etmoxir (#11969) was purchased from Cayman Chemical (Ann Arbor, MI, USA)

### *Statistical analysis*

Continuous variables were tested using Student's t-test. Survival analyses were conducted by the log-rank test using EZR version 1.36 (Saitama Medical Center, Jichi Medical University, Saitama, Japan) [65]. A two-sided P value of $< 0.05$ indicated statistical significance.

### *Data availability*

All RNA-seq datasets were deposited to the DNA Data Bank of Japan (DDBJ; https://wwwddbj.nig.ac.jp/index-e.html) under the accession number: DRA016912.


### Acknowledgments

We thank Paul M. Lieberman (The Wistar Institute, United States), Hironori Yoshiyama (Shimane University, Japan), Wolfgang Hammerschmidt (Helmholtz Zentrum München, Germany), Henri-Jacques Delecluse (German Cancer Research Center, Germany), Hiroyuki Miyoshi (RIKEN, Japan), Yasuo Ariumi (Kumamoto University, Japan), Bob Weinberg (Whitehead Institute for Biomedical Research, United States), Daniel Hodson (University of Cambridge, United Kingdom) and Didier Trono (Ecole Polytechnique Fédérale de Lausanne, Switzerland) for providing invaluable materials. We thank

Tomoko Kunogi, Nobuaki Misawa, Junko Kishikawa, and Shiori Endo (Nagoya University) for technical support; and the Division for Medical Research Engineering at Nagoya University Graduate School of Medicine for technical support of flow cytometry.

## Funding

This work was supported in part by grants from the Japan Society for the Promotion of Science (JSPS) KAKENHI (Grant Numbers JP23K06559 to Y.S., JP23H02723 to H.Kimura., and JP22H02878 to Y.O.); the Japan Science and Technology Agency (JST) PRESTO (Grant Number JPMJPR19H5 to Y.S.), and CREST (Grant Number JPMJCR19H4 to Y.S. and S.T.); the Japan Agency for Medical Research and Development (AMED) (JP21wm0325042 to Y.S.); the Chemo-Sero-Therapeutic Research Institute to H.K.; the Aichi Health Promotion Foundation to K.S.

The funders had no role in study design, data collection and analysis, decision to publish, or preparation of the manuscript.

## Competing interests

H.Kiyoi has received research funding from FUJIFILM, Kyowa-Kirin, Bristol-Myers Squibb, Otsuka, Perseus Proteomics, Daiichi Sankyo, Abbvie, CURED, Astellas Pharma, Chugai, Zenyaku Kogyo, Nippon Shinyaku, Eisai, Takeda, Sumitomo Dainippon Pharma, and Sanofi, in addition to honoraria from Abbvie, Chugai, Astellas Pharma, and Novartis. Other authors declare no competing financial interests.

## Author Contributions

Conceptualization, K.S. and Y.S.; Investigation, K.S., Y.S., Y.O., T.K., T.I., and Y.M.; Data curation, K.S., Y.S. and Y.O.; Resources, T.I., T.M., and S.T.; Supervision, Y.S., H.Kiyoi and H.Kimura; Writing-Original Draft Preparation, K.S., Y.S. and H.Kimura; Writing-Review & Editing, all authors.

## References


1. Young LS, Rickinson AB. Epstein-Barr virus: 40 years on. Nature reviews Cancer. 2004;4(10):757-68. doi: 10.1038/NRC1452.

2. Cohen JI, Fauci AS, Varmus H, Nabel GJ. Epstein-Barr virus: an important vaccine target for cancer prevention. Science translational medicine. 2011;3(107). doi: 10.1126/SCITRANSLMED.3002878.

3. Ma Y, Walsh MJ, Bernhardt K, Ashbaugh CW, Trudeau SJ, Ashbaugh IY, et al. CRISPR/Cas9 Screens Reveal Epstein-Barr Virus-Transformed B Cell Host Dependency Factors. Cell host & microbe. 2017;21(5):580-91.e7. doi: 10.1016/J.CHOM.2017.04.005.

4. Manners O, Murphy JC, Coleman A, Hughes DJ, Whitehouse A. Contribution of the KSHV and EBV lytic cycles to tumourigenesis. Current opinion in virology. 2018;32:60-70. doi: 10.1016/J.COVIRO.2018.08.014.

5. Murata T, Okuno Y, Sato Y, Watanabe T, Kimura H. Oncogenesis of CAEBV revealed: Intragenic deletions in the viral genome and leaky expression of lytic genes. Reviews in medical virology. 2020;30(2). doi: 10.1002/RMV.2095.

6. Münz C. Latency and lytic replication in Epstein-Barr virus-associated oncogenesis. Nature reviews Microbiology. 2019;17(11):691-700. doi: 10.1038/S41579-019-0249-7.

7. Johannsen E, Luftig M, Chase MR, Weicksel S, Cahir-McFarland E, Illanes D, et al. Proteins of purified Epstein-Barr virus. Proceedings of the National Academy of Sciences of the United States of America. 2004;101(46):16286-91. doi: 10.1073/PNAS.0407320101.

8. Full F, Jungnickl D, Reuter N, Bogner E, Brulois K, Scholz B, et al. Kaposi's sarcoma associated herpesvirus tegument protein ORF75 is essential for viral lytic replication and plays a critical role in the antagonization of ND10-instituted intrinsic immunity. PLoS pathogens. 2014;10(1). doi: 10.1371/JOURNAL.PPAT.1003863.

9. Tsai K, Thikmyanova N, Wojcechowskyj JA, Delecluse HJ, Lieberman PM. EBV tegument protein BNRF1 disrupts DAXX-ATRX to activate viral early gene transcription. PLoS pathogens. 2011;7(11). doi: 10.1371/JOURNAL.PPAT.1002376.

10. Feederle R, Neuhierl B, Baldwin G, Bannert H, Hub B, Mautner J, et al. Epstein-Barr Virus BNRF1 Protein Allows Efficient Transfer from the Endosomal Compartment to the Nucleus of Primary B Lymphocytes. Journal of Virology. 2006;80(19):9435-43. doi: 10.1128/jvi.00473-06.

11. Yiu SPT, Guo R, Zerbe C, Weekes MP, Gewurz BE. Epstein-Barr virus BNRF1 destabilizes SMC5/6 cohesin complexes to evade its restriction of replication compartments. Cell reports.

2022;38(10). doi: 10.1016/J.CELREP.2022.110411.
12. Shumilov A, Tsai MH, Schlosser YT, Kratz AS, Bernhardt K, Fink S, et al. Epstein-Barr virus particles induce centrosome amplification and chromosomal instability. Nature Communications. 2017;8. doi: 10.1038/ncomms14257.
13. Santaguida S, Amon A. Short- and long-term effects of chromosome mis-segregation and aneuploidy. Nature reviews Molecular cell biology. 2015;16(8):473-85. doi: 10.1038/NRM4025.
14. Lao M, Zhang X, Ma T, Xu J, Yang H, Duan Y, et al. Regulator of calcineurin 1 gene isoform 4 in pancreatic ductal adenocarcinoma regulates the progression of tumor cells. Oncogene. 2021;40(17):3136-51. doi: 10.1038/S41388-021-01763-Z.
15. Zhang Y, Chen C, Liu Z, Guo H, Lu W, Hu W, et al. PABPC1-induced stabilization of IFI27 mRNA promotes angiogenesis and malignant progression in esophageal squamous cell carcinoma through exosomal miRNA-21-5p. Journal of experimental & clinical cancer research : CR. 2022;41(1). doi: 10.1186/S13046-022-02339-9.
16. Li T, Zhou J, Jiang Y, Zhao Y, Huang J, Li W, et al. The Novel Protein ADAMTS16 Promotes Gastric Carcinogenesis by Targeting IFI27 through the NF-κb Signaling Pathway. International journal of molecular sciences. 2022;23(19). doi: 10.3390/IJMS231911022.
17. Wang H, Qiu X, Lin S, Chen X, Wang T, Liao T. Knockdown of IFI27 inhibits cell proliferation and invasion in oral squamous cell carcinoma. World journal of surgical oncology. 2018;16(1). doi: 10.1186/S12957-018-1371-0.
18. Chiang KC, Huang ST, Wu RC, Huang SC, Yeh TS, Chen MH, et al. Interferon α-inducible protein 27 is an oncogene and highly expressed in cholangiocarcinoma patients with poor survival. Cancer management and research. 2019;11:1893-905. doi: 10.2147/CMAR.S196485.
19. Xu L, Zu T, Li T, Li M, Mi J, Bai F, et al. ATF3 downmodulates its new targets IFI6 and IFI27 to suppress the growth and migration of tongue squamous cell carcinoma cells. PLoS genetics. 2021;17(2). doi: 10.1371/JOURNAL.PGEN.1009283.
20. Okuno Y, Murata T, Sato Y, Muramatsu H, Ito Y, Watanabe T, et al. Defective Epstein-Barr virus in chronic active infection and haematological malignancy. Nature microbiology. 2019;4(3):404-13. doi: 10.1038/S41564-018-0334-0.
21. Davies ML, Xu S, Lyons-Weiler J, Rosendorff A, Webber SA, Wasil LR, et al. Cellular factors associated with latency and spontaneous Epstein-Barr virus reactivation in B-lymphoblastoid cell lines. Virology. 2010;400(1):53-67. doi: 10.1016/J.VIROL.2010.01.002.
22. Meng Q, Hagemeier SR, Fingeroth JD, Gershburg E, Pagano JS, Kenney SC. The Epstein-Barr virus (EBV)-encoded protein kinase, EBV-PK, but not the thymidine kinase (EBV-TK), is

required for ganciclovir and acyclovir inhibition of lytic viral production. J Virol. 2010;84(9):4534-42. Epub 20100224. doi: 10.1128/JVI.02487-09. PubMed PMID: 20181711; PubMed Central PMCID: PMCPMC2863746.

23. Yanagi Y, Okuno Y, Narita Y, Masud H, Watanabe T, Sato Y, et al. RNAseq analysis identifies involvement of EBNA2 in PD-L1 induction during Epstein-Barr virus infection of primary B cells. Virology. 2021;557:44-54. Epub 20210221. doi: 10.1016/j.virol.2021.02.004. PubMed PMID: 33639481.

24. Tang Z, Kang B, Li C, Chen T, Zhang Z. GEPIA2: an enhanced web server for large-scale expression profiling and interactive analysis. Nucleic acids research. 2019;47(W1):W556-W60. doi: 10.1093/NAR/GKZ430.

25. Cheon H, Stark GR. Unphosphorylated STAT1 prolongs the expression of interferon-induced immune regulatory genes. Proc Natl Acad Sci U S A. 2009;106(23):9373-8. Epub 20090528. doi: 10.1073/pnas.0903487106. PubMed PMID: 19478064; PubMed Central PMCID: PMCPMC2688000.

26. Wood VH, O'Neil JD, Wei W, Stewart SE, Dawson CW, Young LS. Epstein-Barr virus-encoded EBNA1 regulates cellular gene transcription and modulates the STAT1 and TGFbeta signaling pathways. Oncogene. 2007;26(28):4135-47. Epub 20070507. doi: 10.1038/sj.onc.1210496. PubMed PMID: 17486072.

27. Najjar I, Baran-Marszak F, Le Clorennec C, Laguillier C, Schischmanoff O, Youlyouz-Marfak I, et al. Latent membrane protein 1 regulates STAT1 through NF-kappaB-dependent interferon secretion in Epstein-Barr virus-immortalized B cells. J Virol. 2005;79(8):4936-43. doi: 10.1128/JVI.79.8.4936-4943.2005. PubMed PMID: 15795279; PubMed Central PMCID: PMCPMC1069527.

28. McLaren JE, Zuo J, Grimstead J, Poghosyan Z, Bell AI, Rowe M, et al. STAT1 contributes to the maintenance of the latency III viral programme observed in Epstein-Barr virus-transformed B cells and their recognition by CD8+ T cells. J Gen Virol. 2009;90(Pt 9):2239-50. Epub 20090513. doi: 10.1099/vir.0.011627-0. PubMed PMID: 19439556.

29. Cui X, Liu H, Shi T, Zhao Q, Li F, Lv W, et al. IFI27 Integrates Succinate and Fatty Acid Oxidation to Promote Adipocyte Thermogenic Adaption. Adv Sci (Weinh). 2023;10(28):e2301855. Epub 20230806. doi: 10.1002/advs.202301855. PubMed PMID: 37544897; PubMed Central PMCID: PMCPMC10558685.

30. Murphy MP. How mitochondria produce reactive oxygen species. Biochem J. 2009;417(1):1-13. doi: 10.1042/BJ20081386. PubMed PMID: 19061483; PubMed Central PMCID:

599 PMCPMC2605959.
600 31. Giorgio M, Trinei M, Migliaccio E, Pelicci PG. Hydrogen peroxide: a metabolic by-product
601 or a common mediator of ageing signals? Nat Rev Mol Cell Biol. 2007;8(9):722-8. doi:
602 10.1038/nrm2240. PubMed PMID: 17700625.
603 32. Speijer D. Molecular characteristics of the multi-functional FAO enzyme ACAD9 illustrate
604 the importance of FADH(2) /NADH ratios for mitochondrial ROS formation. Bioessays.
605 2022;44(8):e2200056. Epub 20220616. doi: 10.1002/bies.202200056. PubMed PMID: 35708204.
606 33. Orrenius S, Gogvadze V, Zhivotovsky B. Mitochondrial oxidative stress: implications for
607 cell death. Annu Rev Pharmacol Toxicol. 2007;47:143-83. doi:
608 10.1146/annurev.pharmtox.47.120505.105122. PubMed PMID: 17029566.
609 34. Yao CH, Liu GY, Wang R, Moon SH, Gross RW, Patti GJ. Identifying off-target effects of
610 etomoxir reveals that carnitine palmitoyltransferase I is essential for cancer cell proliferation
611 independent of beta-oxidation. PLoS Biol. 2018;16(3):e2003782. Epub 20180329. doi:
612 10.1371/journal.pbio.2003782. PubMed PMID: 29596410; PubMed Central PMCID:
613 PMCPMC5892939.
614 35. Hong GK, Gulley ML, Feng W-H, Delecluse H-J, Holley-Guthrie E, Kenney SC. Epstein-
615 Barr virus lytic infection contributes to lymphoproliferative disease in a SCID mouse model. Journal
616 of virology. 2005;79(22):13993-4003. doi: 10.1128/JVI.79.22.13993-14003.2005.
617 36. Okuno Y, Murata T, Sato Y, Muramatsu H, Ito Y, Watanabe T, et al. Publisher Correction:
618 Defective Epstein-Barr virus in chronic active infection and haematological malignancy. Nat
619 Microbiol. 2019;4(3):544. doi: 10.1038/s41564-019-0387-8. PubMed PMID: 30705423.
620 37. Wyżewski Z, Mielcarska MB, Gregorczyk-Zboroch KP, Myszka A. Virus-Mediated
621 Inhibition of Apoptosis in the Context of EBV-Associated Diseases: Molecular Mechanisms and
622 Therapeutic Perspectives. International journal of molecular sciences. 2022;23(13). doi:
623 10.3390/IJMS23137265.
624 38. Nishiu M, Tomita Y, Nakatsuka SI, Takakuwa T, Iizuka N, Hoshida Y, et al. Distinct pattern
625 of gene expression in pyothorax-associated lymphoma (PAL), a lymphoma developing in long-
626 standing inflammation. Cancer science. 2004;95(10):828-34. doi: 10.1111/J.1349-
627 7006.2004.TB02189.X.
628 39. Cheriyath V, Leaman DW, Borden EC. Emerging roles of FAM14 family members
629 (G1P3/ISG 6-16 and ISG12/IFI27) in innate immunity and cancer. Journal of interferon & cytokine
630 research : the official journal of the International Society for Interferon and Cytokine Research.
631 2011;31(1):173-81. doi: 10.1089/JIR.2010.0105.

632 40. Rosebeck S, Leaman DW. Mitochondrial localization and pro-apoptotic effects of the
633 interferon-inducible protein ISG12a. Apoptosis. 2008;13(4):562-72. doi: 10.1007/S10495-008-0190-
634 0/METRICS.
635 41. Martensen PM, Søgaard TMM, Gjermandsen IM, Buttenschøn HN, Rossing AB, Bonnevie-
636 Nielsen V, et al. The interferon alpha induced protein ISG12 is localized to the nuclear membrane.
637 European journal of biochemistry. 2001;268(22):5947-54. doi: 10.1046/J.0014-2956.2001.02545.X.
638 42. Gytz H, Hansen MF, Skovbjerg S, Kristensen ACM, Hørlyck S, Jensen MB, et al. Apoptotic
639 properties of the type 1 interferon induced family of human mitochondrial membrane ISG12 proteins.
640 Biology of the cell. 2017;109(2):94-112. doi: 10.1111/BOC.201600034.
641 43. Henderson S, Rowe M, Gregory C, Croom-Carter D, Wang F, Longnecker R, et al. Induction
642 of bcl-2 expression by Epstein-Barr virus latent membrane protein 1 protects infected B cells from
643 programmed cell death. Cell. 1991;65(7):1107-15. doi: 10.1016/0092-8674(91)90007-L.
644 44. Kvansakul M, Wei AH, Fletcher JI, Willis SN, Chen L, Roberts AW, et al. Structural basis
645 for apoptosis inhibition by Epstein-Barr virus BHRF1. PLoS pathogens. 2010;6(12). doi:
646 10.1371/JOURNAL.PPAT.1001236.
647 45. Bellows DS, Howell M, Pearson C, Hazlewood SA, Hardwick JM. Epstein-Barr virus
648 BALF1 is a BCL-2-like antagonist of the herpesvirus antiapoptotic BCL-2 proteins. Journal of
649 virology. 2002;76(5):2469-79. doi: 10.1128/JVI.76.5.2469-2479.2002.
650 46. Jin W, Jin W, Pan D. Ifi27 is indispensable for mitochondrial function and browning in
651 adipocytes. Biochem Biophys Res Commun. 2018;501(1):273-9. Epub 20180508. doi:
652 10.1016/j.bbrc.2018.04.234. PubMed PMID: 29730295.
653 47. Yu T, Robotham JL, Yoon Y. Increased production of reactive oxygen species in
654 hyperglycemic conditions requires dynamic change of mitochondrial morphology. Proc Natl Acad Sci
655 U S A. 2006;103(8):2653-8. Epub 20060213. doi: 10.1073/pnas.0511154103. PubMed PMID:
656 16477035; PubMed Central PMCID: PMCPMC1413838.
657 48. Mentzer AJ, Brenner N, Allen N, Littlejohns TJ, Chong AY, Cortes A, et al. Identification
658 of host-pathogen-disease relationships using a scalable multiplex serology platform in UK Biobank.
659 Nature communications. 2022;13(1). doi: 10.1038/S41467-022-29307-3.
660 49. Adhikary D, Damaschke J, Mautner J, Behrends U. The Epstein-Barr Virus Major Tegument
661 Protein BNRF1 Is a Common Target of Cytotoxic CD4+ T Cells. Journal of virology. 2020;94(15).
662 doi: 10.1128/JVI.00284-20.
663 50. Abbott RJM, Quinn LL, Leese AM, Scholes HM, Pachnio A, Rickinson AB. CD8 + T Cell
664 Responses to Lytic EBV Infection: Late Antigen Specificities as Subdominant Components of the

665 Total Response. The Journal of Immunology. 2013;191(11):5398-409. doi:
666 10.4049/jimmunol.1301629.
667 51. Djavadian R, Hayes M, Johannsen E. CAGE-seq analysis of Epstein-Barr virus lytic gene
668 transcription: 3 kinetic classes from 2 mechanisms. PLoS pathogens. 2018;14(6). doi:
669 10.1371/JOURNAL.PPAT.1007114.
670 52. Sato Y, Yaguchi M, Okuno Y, Ishimaru H, Sagou K, Ozaki S, et al. Epstein-Barr virus
671 tegument protein BGLF2 in exosomes released from virus-producing cells facilitates de novo infection.
672 Cell communication and signaling : CCS. 2022;20(1). doi: 10.1186/S12964-022-00902-7.
673 53. Yanagi Y, Watanabe T, Hara Y, Sato Y, Kimura H, Murata T. EBV Exploits RNA m(6)A
674 Modification to Promote Cell Survival and Progeny Virus Production During Lytic Cycle. Front
675 Microbiol. 2022;13:870816. Epub 20220615. doi: 10.3389/fmicb.2022.870816. PubMed PMID:
676 35783391; PubMed Central PMCID: PMCPMC9240777.
677 54. Katsumura KR, Maruo S, Wu Y, Kanda T, Takada K. Quantitative evaluation of the role of
678 Epstein-Barr virus immediate-early protein BZLF1 in B-cell transformation. J Gen Virol. 2009;90(Pt
679 10):2331-41. doi: 10.1099/vir.0.012831-0. PubMed PMID: 19553389.
680 55. Sato Y, Yaguchi M, Okuno Y, Ishimaru H, Sagou K, Ozaki S, et al. Epstein-Barr virus
681 tegument protein BGLF2 in exosomes released from virus-producing cells facilitates de novo infection.
682 Cell Commun Signal. 2022;20(1):95. Epub 20220621. doi: 10.1186/s12964-022-00902-7. PubMed
683 PMID: 35729616; PubMed Central PMCID: PMCPMC9210680.
684 56. Murata T, Isomura H, Yamashita Y, Toyama S, Sato Y, Nakayama S, et al. Efficient
685 production of infectious viruses requires enzymatic activity of Epstein-Barr virus protein kinase.
686 Virology. 2009;389(1-2):75-81. doi: 10.1016/J.VIROL.2009.04.007.
687 57. Delecluse HJ, Hilsendegen T, Pich D, Zeidler R, Hammerschmidt W. Propagation and
688 recovery of intact, infectious Epstein-Barr virus from prokaryotic to human cells. Proceedings of the
689 National Academy of Sciences of the United States of America. 1998;95(14):8245-50. doi:
690 10.1073/PNAS.95.14.8245/ASSET/ED6EF4C8-7CE9-49B0-9BC4-
691 4A552469F3B4/ASSETS/GRAPHIC/PQ1381539006.JPEG.
692 58. Inagaki T, Sato Y, Ito J, Takaki M, Okuno Y, Yaguchi M, et al. Direct Evidence of Abortive
693 Lytic Infection-Mediated Establishment of Epstein-Barr Virus Latency During B-Cell Infection.
694 Frontiers in microbiology. 2021;11. doi: 10.3389/FMICB.2020.575255.
695 59. Sato Y, Kamura T, Shirata N, Murata T, Kudoh A, Iwahori S, et al. Degradation of
696 phosphorylated p53 by viral protein-ECS E3 ligase complex. PLoS pathogens. 2009;5(7). doi:
697 10.1371/JOURNAL.PPAT.1000530.

60. Tsai K, Chan L, Gibeault R, Conn K, Dheekollu J, Domsic J, et al. Viral Reprogramming of the Daxx Histone H3.3 Chaperone during Early Epstein-Barr Virus Infection. Journal of Virology. 2014;88(24):14350-63. doi: 10.1128/jvi.01895-14.

61. Suzuki T, Sato Y, Okuno Y, Goshima F, Mikami T, Umeda M, et al. Genome-wide CRISPR screen for HSV-1 host factors reveals PAPSS1 contributes to heparan sulfate synthesis. Communications biology. 2022;5(1). doi: 10.1038/S42003-022-03581-9.

62. Narita Y, Murata T, Ryo A, Kawashima D, Sugimoto A, Kanda T, et al. Pin1 Interacts with the Epstein-Barr Virus DNA Polymerase Catalytic Subunit and Regulates Viral DNA Replication. Journal of Virology. 2013;87(4):2120-7. doi: 10.1128/JVI.02634-12.

63. Murata T, Noda C, Narita Y, Watanabe T, Yoshida M, Ashio K, et al. Induction of Epstein-Barr Virus Oncoprotein LMP1 by Transcription Factors AP-2 and Early B Cell Factor. Journal of Virology. 2016;90(8):3873-89. doi: 10.1128/JVI.03227-15/ASSET/3C791E4C-44CC-409B-9523-EC61CF3D8CF9/ASSETS/GRAPHIC/ZJV9990915200010.JPEG.

64. Okuno Y, Murata T, Sato Y, Muramatsu H, Ito Y, Watanabe T, et al. Defective Epstein-Barr virus in chronic active infection and haematological malignancy. Nat Microbiol. 2019;4(3):404-13. Epub 2019/01/22. doi: 10.1038/s41564-018-0334-0. PubMed PMID: 30664667.

65. Kanda Y. Investigation of the freely available easy-to-use software 'EZR' for medical statistics. Bone Marrow Transplantation. 2013;48(3):452-8.

## Figure Legends

Fig. 1

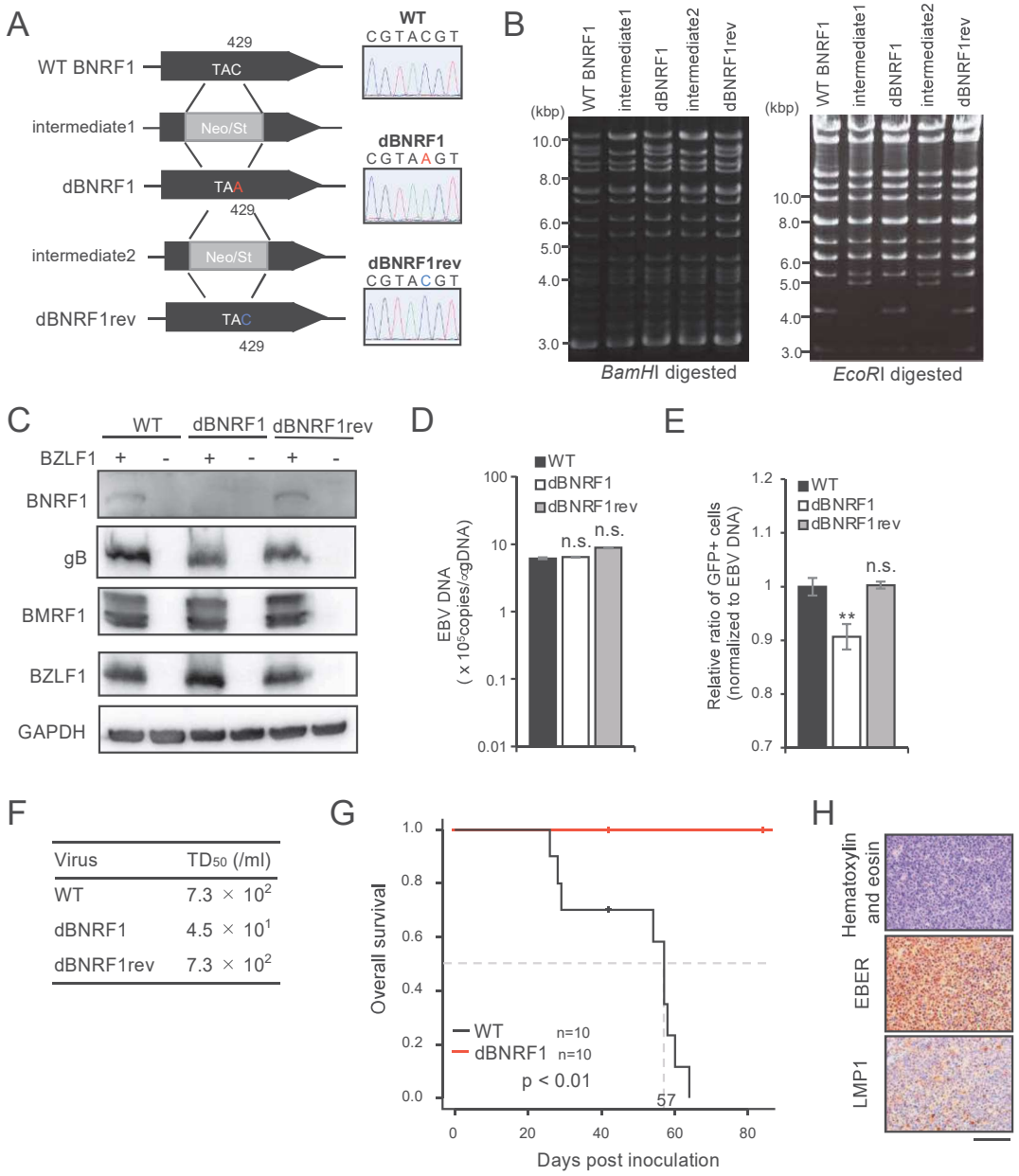


**Fig. 1. Characterization of BNRF1-KO EBV.**

(A) Schematic diagrams of BNRF1-KO recombinant viruses used in this study. The Neo/St cassette containing the neomycin resistance and streptomycin sensitivity genes was inserted between nucleotides 312 and 738 of the BNRF1 gene to prepare an intermediate, and the C429A (stop codon) mutation was introduced when this cassette was removed (dBNRF1). The Neo/St cassette was reinserted to the same position of

dBNRF1 (intermediate 2), and then A429 was replaced with C when this cassette was removed (dBNRF1rev). Successful recombination was confirmed by Sanger sequencing as presented in the right panels.

(B) Electrophoresis of EBV-BAC digested with *BamH*I (left) or *EcoR*I (right).

(C) Immunoblots of lysates from HEK293T cells carrying the indicated EBV-BAC with or without pcDNA-BZLF1 transfection with the indicated antibodies.

(D) Quantification of viral genomic DNA in HEK293T cells carrying the indicated recombinant EBV-BAC genomes at 72 h after pcDNA-BZLF1 transfection. The results in the bar graphs are presented as the mean ± SD. n.s., not significant.

(E) Virus titers in 100 μL of supernatants were determined by counting the proportion of EGFP-positive Akata(-) cells by flow cytometry 2 days after infection. The results in the bar graphs are presented as the mean ± SD. ** $p < 0.01$ compared to WT.

(F) PBMCs were infected with 10-fold serial dilutions of the indicated EBV. After 3 weeks, the transformation efficiency ($TD_{50}$/mL) was calculated by examining the number of wells in which clumps of LCLs were present.

(G) The pathogenicity of LCLs in vivo. Overall survival for 6-week-old mice inoculated with LCLs-WT or LCLs-dBNRF1. The 50% survival was 57 days in LCLs-WT.

(H) Histochemistry of the intraperitoneal tumors stained with hematoxylin and eosin (top), and analyzed by EBER in situ hybridization (middle) and LMP1 immunohistochemistry (bottom). The images are representative of two independent experiments with similar results. Scale bar, 100 μm.

Fig. 2

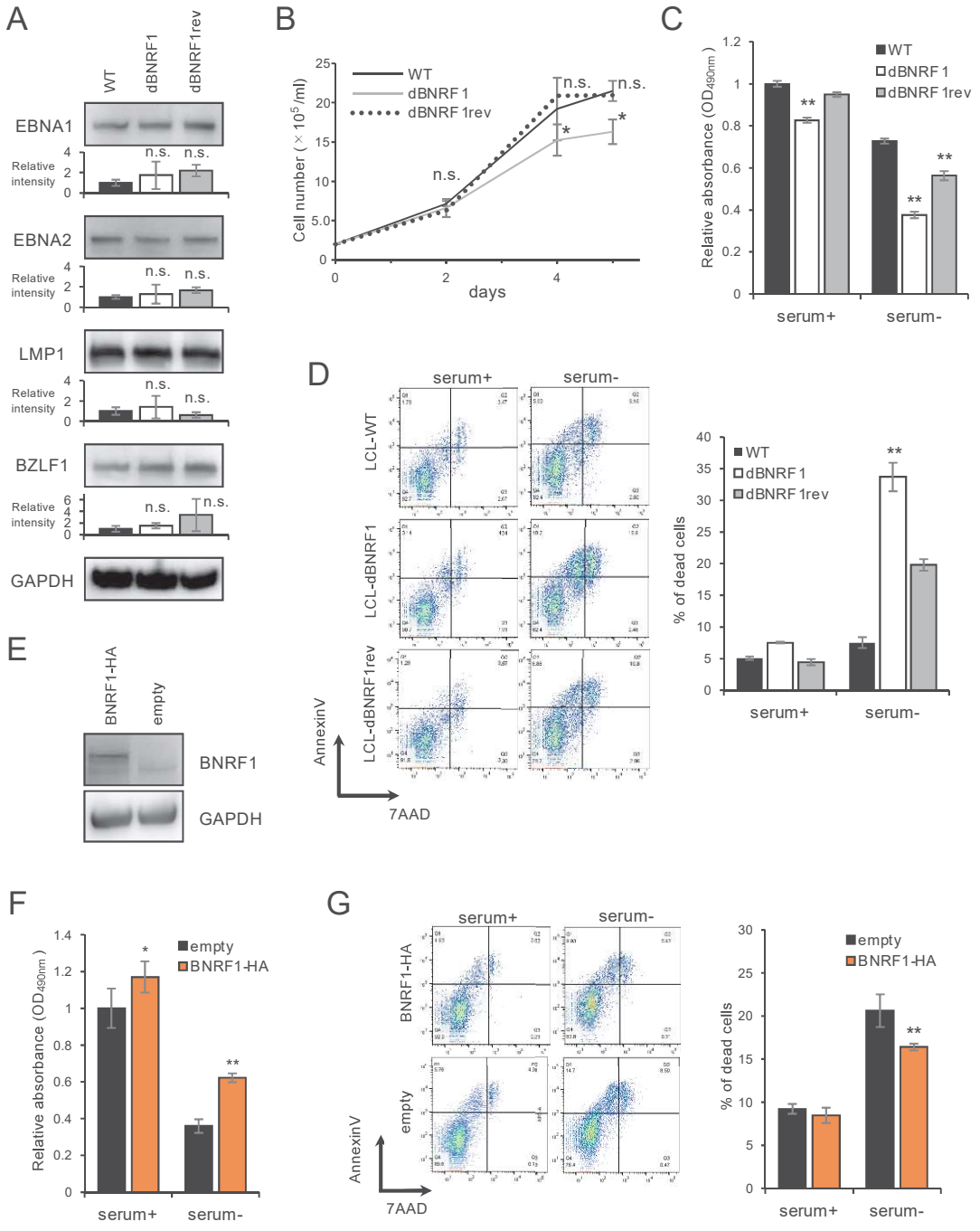


747

748 **Fig. 2.** LCL-dBNRF1 exhibited slower growth than LCLs-WT.

749 (A) Immunoblots of lysates from LCLs-WT, LCLs-dBNRF1, and LCLs-dBNRF1rev

750 with the indicated antibodies. The results in the bar graphs are presented as the relative

751 mean intensity ± SD. n.s., not significant.

752 (B) The growth curves of the indicated LCLs over 5 days after seeding at $2 \times 10^5$ cells.

753 The results are presented as the mean ± SD of three independent experiments. * p <
754 0.05 compared to LCLs-WT.
755 (C) Viability of LCLs cultured with or without serum for 24 h as assessed by the MTS
756 assay. The absorbance at 490 nm is normalized to LCLs-WT cultured in the presence of
757 serum. The results are presented as the mean ± SD. ** p < 0.01 compared to any LCLs
758 with the same condition.
759 (D) Annexin V/7-AAD assay of LCLs with or without serum. LCLs were maintained
760 with or without serum-depleted medium for 24 h and then harvested. Dead cells were
761 defined as those positive for annexin V or both annexin V and 7-AAD. The results in
762 the bar graphs are presented as the mean ± SD. ** p < 0.01 compared to any LCLs
763 without serum.
764 (E) Immunoblots confirming the trans-complementation of BNRF1 in LCLs-dBNRF1.
765 (F) Viability of LCLs-dBNRF1 complemented with BNRF1 with or without serum for
766 24 h as assessed by the MTS assay. The results are presented as the mean ± SD. * p <
767 0.05, ** p < 0.01.
768 (G) Annexin V/7-AAD assay of LCLs-dBNRF1 complemented with BNRF1 with or
769 without serum. Dead cells were defined as those positive for annexin V or both annexin
770 V and 7-AAD. The results are presented as the mean ± SD. ** p < 0.01.
771

Fig. 3

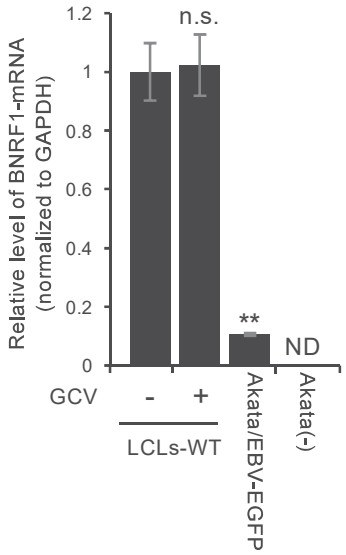


772

773 **Fig. 3. LCLs express BNRF1-mRNA in the latent state.**

774 LCLs-WT was cultured for 48 h with or without 20 μM ganciclovir. Total RNA
775 extracted from the indicated LCLs-WT, Akata/EBV-eGFP cells, and Akata(-) cells was
776 examined by RT-qPCR. The results are presented as the mean ± SD. ** $p < 0.01$, n.s.,
777 not significant, ND, not detected.

Fig. 4

A

LCLs

LCL-WT / LCL-dBNRF1

| gene | log2FC |
|---|---|
| PHYHD1 | 22.61 |
| NLRP2 | 10.60 |
| ZFP57 | 10.28 |
| TAC1 | 9.05 |
| LOC441666 | 8.99 |
| OTOF | 8.53 |
| LHX1 | 6.44 |
| FOXJ1 | 6.36 |
| SOX18 | 6.15 |
| COL1A2 | 5.81 |
| TMPRSS3 | 4.87 |
| LDOC1 | 4.65 |
| IFI27 | 4.57 |
| ZNF831 | 4.42 |
| TMEM163 | 4.33 |
| TRPM2 | 3.85 |
| SPNS3 | 3.71 |
| LINC00176 | 3.71 |
| CABP1 | 3.68 |
| SSH3 | 3.57 |

B

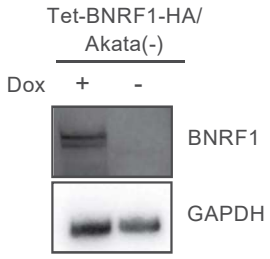


C

Tet-BNRF1-HA/ Akata(-)

Dox+ / Dox-

| gene | log2FC |
|---|---|
| LINC01096 | 8.63 |
| IFI27 | 7.92 |
| IFIT1 | 7.65 |
| ZBP1 | 7.39 |
| IFIT3 | 7.28 |
| RSAD2 | 7.27 |
| NMI | 6.79 |
| MX2 | 6.74 |
| CCR6 | 6.70 |
| CCR1 | 6.70 |
| XAF1 | 6.55 |
| SPATS2L | 6.38 |
| IFI6 | 6.35 |
| OASL | 6.32 |
| DAZL | 6.23 |
| IFNB1 | 6.18 |
| IFIT5 | 5.85 |
| IFI44 | 5.83 |
| SAMD9L | 5.82 |
| OTOF | 5.82 |

D

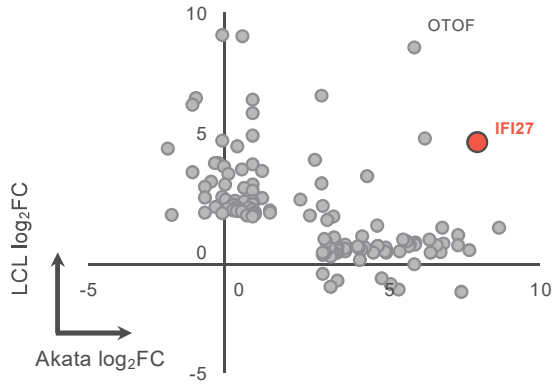


E

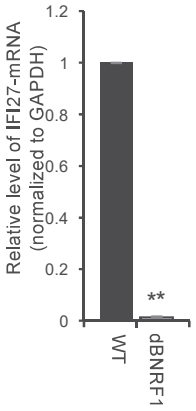


F

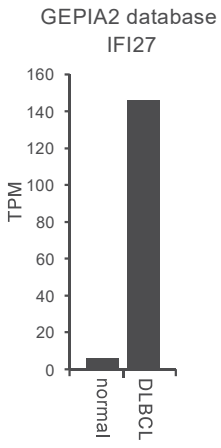


**Fig. 4. RNA-seq analyses of LCLs and Akata(-) cells inducibly expressing BNRF1.**

(A) Upregulated genes in LCLs-WT compared to those in LCLs-dBNRF1 as determined using the $\log_2$ fold-change (FC). The top 20 genes are presented.

(B) Western blotting confirming BNRF1 expression in Tet-BNRF1/Akata(-) cells after the addition of Dox.

(C) Upregulated genes in Tet-BNRF1/Akata(-) cells treated with Dox compared to untreated cells as determined using $\log_2$ FC. The top 20 genes are presented.

(D) Top 120 genes upregulated in LCLs-WT and Tet-BNRF1/Akata(-) cells with Dox are shown in the scatter plot of $\log_2$ FC in LCLs and Tet-BNRF1/Akata(-) cells.

(E) Validation of IFI27 mRNA expression in LCLs. Total RNA extracted from the

789 indicated LCLs was examined by RT-qPCR. The results are presented as the mean ± SD.

790 ** $p < 0.01$.

791 (F) IFI27 mRNA expression in diffuse large B cell lymphoma according to RNA-seq

792 data in the GEPIA2 database.

Fig. 5

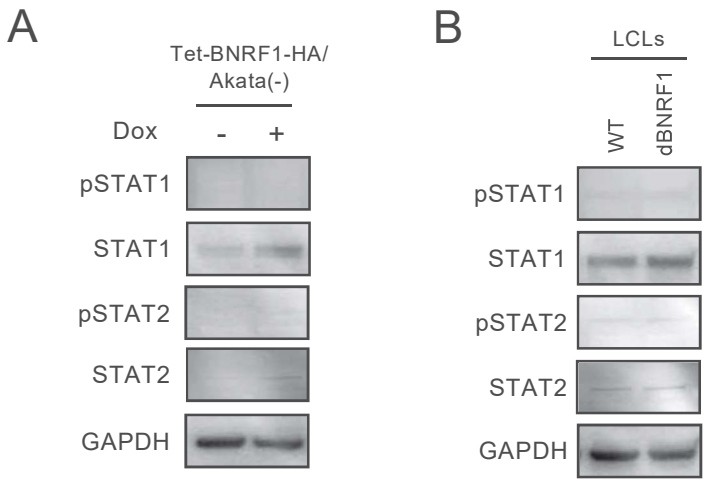


**Fig. 5. The expression of STAT1 and STAT2 in Akata(-) cells inducibly expressing BNRF1 and LCLs.**

(A) Immunoblots of lysates from et-BNRF1/Akata(-) cells cultured with or without Dox with the indicated antibodies.

(B) Immunoblots of lysates from LCLs-WT and LCLs-dBNRF1 with the indicated antibodies.

Fig. 6

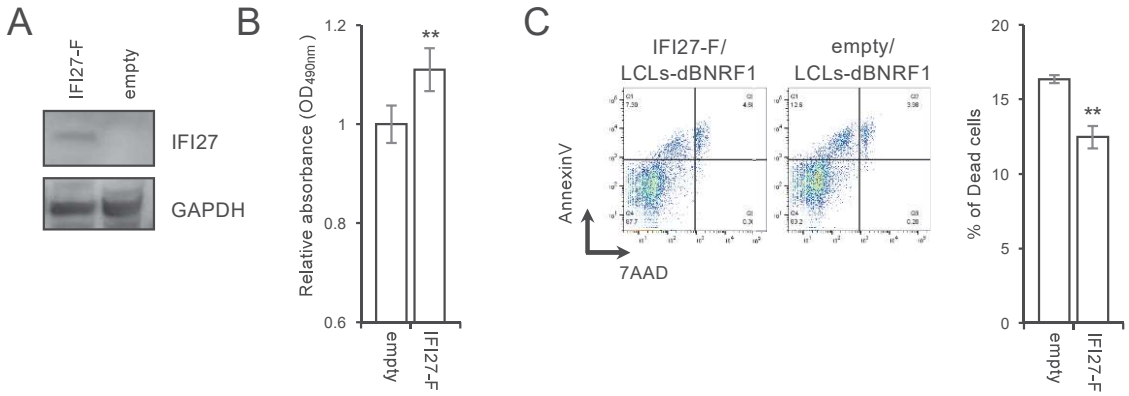


**Fig. 6. IFI27 supports LCL survival.**

(A) Immunoblots confirming the expression of IFI27 tagged with a FLAG epitope (IFI27-F) in LCLs-dBNRF1.

(B) Viability of LCLs-dBNRF1 with or without exogenous IFI27 cultured for 48 h as assessed by the MTS assay. The results are presented as the mean ± SD. ** $p < 0.01$.

(C) Annexin V/7-AAD assay of LCLs-dBNRF1 with or without exogenous IFI27. Dead LCLs were defined as those positive for annexin V or both annexin V and 7-AAD. The results are presented as the mean ± SD. ** $p < 0.01$.

Fig. 7

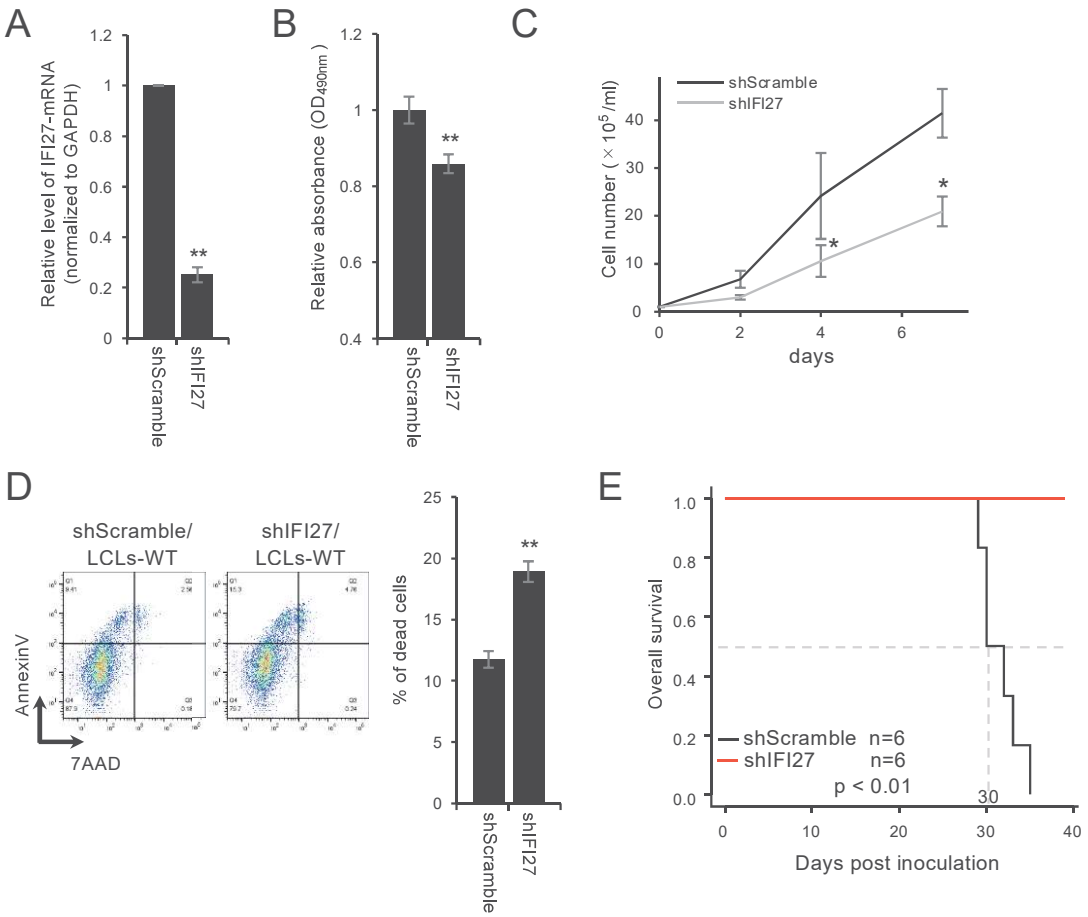


811

812 **Fig. 7. Knockdown of IFI27 impairs LCL survival *in vitro* and *in vivo*.**

813 (A) RT-qPCR confirming the knockdown of IFI27 mRNA in LCLs. LCLs-WT carrying

814 shScramble (shScramble/LCLs-WT) and shIFI27 (shIFI27/LCLs-WT) were established

815 by blasticidin selection after lentiviral-mediated shRNA transduction. The results are

816 presented as the mean ± SD. ** $p < 0.01$.

817 (B) Viability of LCLs-WT carrying shScramble or shIFI27 and cultured for 48 h as

818 assessed by the MTS assay. The results are presented as the mean ± SD. ** $p < 0.01$.

819 (C) The growth curve of LCLs-WT carrying shScramble or shIFI27 over 7 days after

820 seeding at $2 \times 10^5$ cells. The results are presented as the mean ± SD of three

821 independent experiments. * $p < 0.05$.

822 (D) Annexin V/7-AAD assay of LCLs-WT carrying shScramble or shIFI27. Dead LCLs

823 were defined as those positive for annexin V or both annexin V and 7-AAD. The results

824 are presented as the mean ± SD. ** $p < 0.01$.

825 (E) Overall survival of 5-week-old mice inoculated with LCLs-WT carrying

826 shScramble or shIFI27. The 50% survival was 30 days in LCLs-WT/shScramble.

Fig. 8

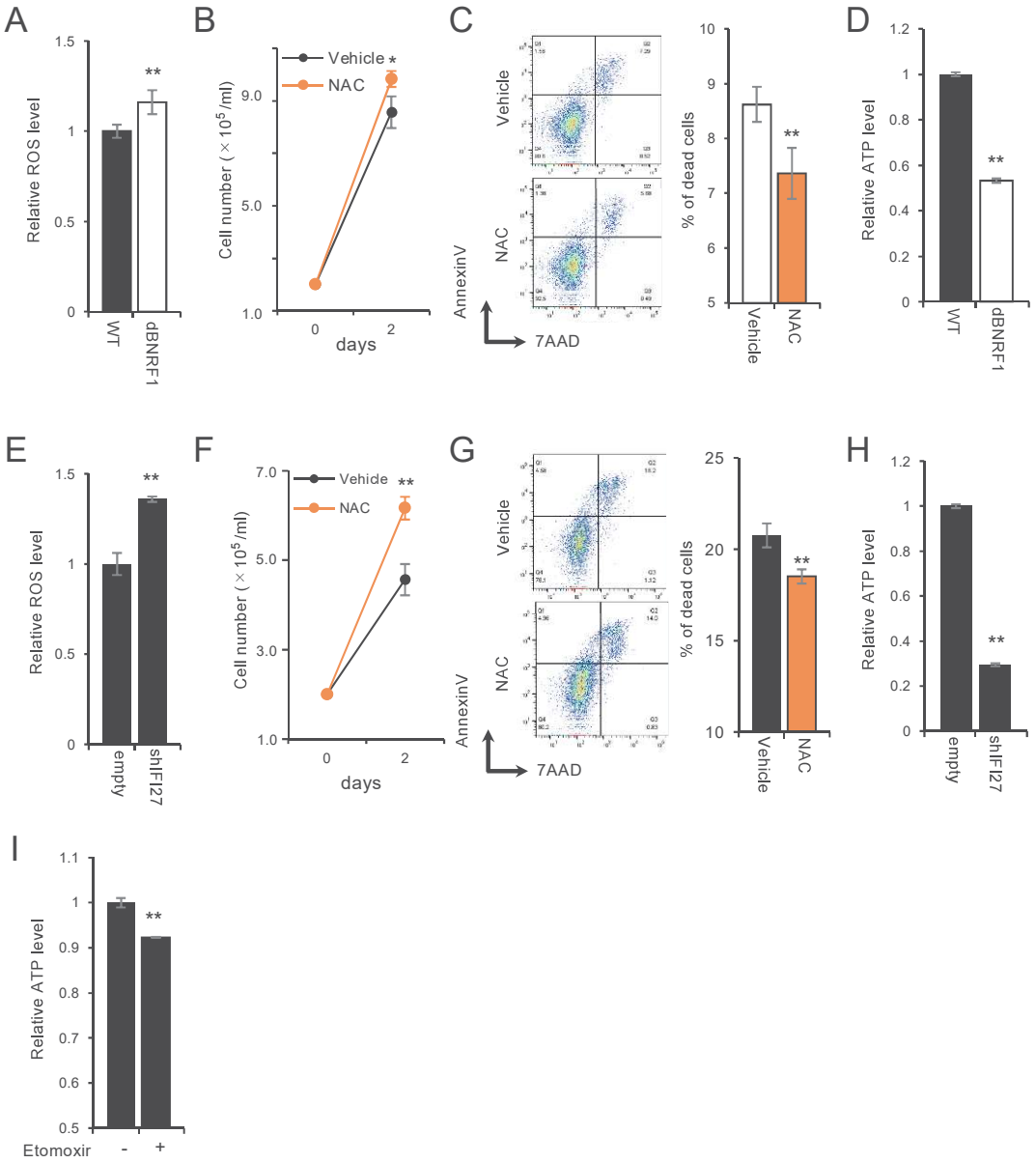


**Fig. 8. BNRF1-KO or IFI27-KD induced ROS production.**

(A and E) The relative ROS production of LCLs-WT and LCLs-dBNRF1 (A), or shScramble/LCLs-WT and shIFI27/LCLs-WT (E). The results are presented as the mean ± SD of three independent experiments. ** $p < 0.01$. (B and F) The growth of LCLs-dBNRF1 (B) or shIFI27/LCLs-WT (F) with or without 2 mM NAC over 2 days after seeding at $2 \times 10^5$ cells. The results are presented as the mean ± SD of three independent experiments. * $p < 0.05$, ** $p < 0.01$.

(C and G) Annexin V/7-AAD assay of LCLs-dBNRF1(C) or shIFI27/LCLs-WT (G) cultured for 48 h in the presence or absence of 2 mM NAC. Dead LCLs were defined as those positive for annexin V or both annexin V and 7-AAD. The results are presented as the mean ± SD. ** $p < 0.01$.

(D and H) The relative ATP production of LCLs-WT and LCLs-dBNRF1 (D), or shScramble/LCLs-WT and shIFI27/LCLs-WT (H). The results are presented as the mean ± SD of three independent experiments. ** $p < 0.01$.

(I) The relative ATP production of LCLs-WT cultured in the presence or absence of 20mM etomoxir. The results are presented as the mean ± SD of three independent experiments. ** $p < 0.01$.

Fig. 9

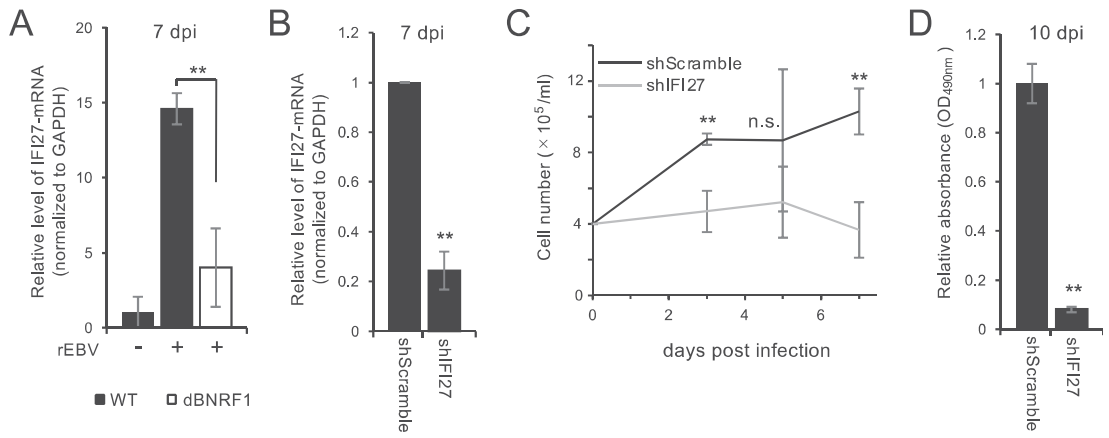


**Fig. 9. Knockdown of IFI27 impairs the proliferation of EBV-infected B cells during de novo infection.**

(A) RT-qPCR of IFI27 mRNA in mock-infected B cells or those infected with EBV-WT or EBV-dBNRF1 at 7 dpi. The results are presented as the mean ± SD. ** $p < 0.01$.

(B) RT-qPCR confirming knockdown of IFI27 mRNA in EBV-infected B cells at 7 dpi. The results are presented as the mean ± SD. ** $p < 0.01$.

(C) Growth curve analyses of B cells carrying the indicated shRNA up to 7 dpi with EBV. Cells were seeded at $4 \times 10^5$ cells. The results are presented as the mean ± SD. ** $p < 0.01$.

(D) Viability of EBV-infected B cells carrying shScramble or shIFI27 at 10 dpi. The results are presented as the mean ± SD. ** $p < 0.01$.

859 Table 1. Oligonucleotides used for the generation of recombinant EBV

| Oligo name | Sequence (5' to 3') |
|---|---|
| BNRF1-NeoSt-pF | GGCCCTCGTTGGCATTCTACTAGGAAACGGCGACAGG GTGAACACTTGGGCACGGAGAGGGCCTGGTGATGATG GCGGGATC |
| BNRF1-NeoSt-pR | CAAGTGGCCCGAGTAAGTGTCTCGCAGCGCGGACACG ATCTTAGCTCGTCGGCCAGCTGTCGGAAGAACTCGTC AAGAAGG |
| BNRF1-stop-pF | GGCGCCACGTAAGTGCTTCGCG |
| BNRF1-stop-pR | CGCGAAGCACTTACGTGGCGCC |
| BNRF1-rev-pF | GGCCCTCGTTGGCATTCTAC |
| BNRF1-rev-pR | CAAGTGGCCCGAGTAAGTGTC |

860

861 Table 2. Primers used for RT-qPCR

| Primer name | Sequence (5' to 3') |
|---|---|
| IFI27-F | CGTCCTCCATAGCAGCCAAGAT |
| IFI27-R | ACCCAATGGAGCCCAGGATGAA |
| BNRF1-F | CAGAGACCGCTGACACGAGG |
| BNRF1-R | CTGAAGGACCAAGTGGCCCG |
| GAPDH-F | GTCTCCTCTGACTTCAACAGCG |
| GAPDH-R | ACCACCCTGTTGCTGTAGCCAA |

862